Inorganic Chemistry
Article

Inorg. Chem. **2009**, *48*, 8493–8507 **8493**
DOI: 10.1021/ic9012153

Sitting-Atop Metallo-Porphyrin Complexes: Experimental and Theoretical Investigations on Such Elusive Species

Giovanna De Luca,[†] Andrea Romeo,[†] Luigi Monsù Scolaro,*[,†] Giampaolo Ricciardi,[‡] and Angela Rosa*[,‡]

[†]*Dipartimento di Chimica Inorganica, Chimica Analitica e Chimica Fisica, Università di Messina, and C.I.R.C.M.S.B., Salita Sperone 31, Vill. S. Agata, Messina, Italy, and* [‡]*Dipartimento di Chimica, Università della Basilicata, Via N. Sauro 85, 85100 Potenza, Italy*

Received June 24, 2009

The interaction between the sodium cation and two *meso*-aryl porphyrins (tetraphenylporphyrin, TPP, and tetra(4-methoxyphenyl)porphyrin, TMPP) leads to the formation of new species that have been identified as Sitting-Atop (SAT) complexes, where the metal ion interacts with the N atoms of the porphyrin core without the concomitant deprotonation of the N−H groups. These species have been attained in low polarity solvent through the interaction of the porphyrin free bases with sodium tetrakis[3,5-bis(trifluoromethyl)phenyl]borate (NaTFPB), and investigated in situ through a combination of spectroscopic techniques, such as UV/vis absorption and fluorescence (static and time-resolved), resonance light scattering, FT-IR, and ^{1}H NMR. All spectroscopic evidence points to the occurrence of a single equilibrium between each parent compound and its SAT complex, ruling out the presence of other metallo-, protonated, or aggregated porphyrins in solution. The 1:1 stoichiometry of the adducts has been determined via continuous variation method (Job's plot), and an estimate of the corresponding association constants in CH_2Cl_2 at 298 K have been obtained by UV/vis titration ($K_{eq} = (9 \pm 4) \times 10^5$ L mol^{-1} and $(5 \pm 2) \times 10^6$ L mol^{-1} for TPP and TMPP, respectively). Density-functional theory (DFT) calculations on SAT model complexes, [NaTPP(PF_6)] and [NaTMPP(PF_6)], have provided information on the molecular structure of these elusive species and on the nature and strength of the sodium−porphyrin interaction. It is found that the sodium ion is bound to the four nitrogen atoms of the porphyrin core. The involvement of the pyrrolic N atoms results in a modest but not negligible elongation of the N−H bonds, pyramidalization of the hydrogen atoms, and blue shift of the N−H stretching frequencies. Electronic structure and energy decomposition analysis reveal that covalent interactions, mainly consisting of porphyrin to sodium charge transfer interactions, are an important component of the sodium-porphyrin bond. Time-dependent DFT (TDDFT) calculations of the lowest excited states of the model systems provide an unambiguous interpretation of the absorption and emission properties of the experimentally identified SAT complexes.

Introduction

Porphyrins constitute an important class of natural and synthetic pigments having a wide role in biological processes and in technological applications. In Nature, porphyrin metal-derivatives are the active site of many redox-active enzymes and transport proteins, for example, cytochromes and hemoglobin. In biological systems, the complexation of a metal ion into the macrocyclic core of the porphyrin ring is facilitated by specific enzymes, termed chelatases.[1] In synthetic procedures, metal insertion is generally performed in solution by adding the proper metal ion to the porphyrin in a basic medium, which can be the solvent, for example, dimethylformamide.[2] Considering the importance of these compounds and their biological implications, significant effort has been devoted to elucidating the mechanism of porphyrin metalation. Among the proposed mechanistic pathways, the most debated reaction intermediate is the so-called "sitting-atop" (SAT), which was originally invoked by Fleischer and Wang[3] for the Fe(III) insertion into proto-porphyrin IX (PPIX) dimethyl ester in chloroform. This species was detected in solution for its distinct absorption features with respect to the starting free ligand and the final metal complex. The hypothetical structure proposed for this intermediate displays a rather weak interaction between Fe(III) and the two pyrrolenine nitrogen atoms, to form a chelated ring and leaving unaltered the two pyrrole N−H

*To whom correspondence should be addressed. E-mail: lmonsu@unime.it (L.M.S.), angela.rosa@unibas.it (A.R.). Phone: +39 090 676 5711 (L.M.S.), (+)39 0971 202238 (A.R.). Fax: +39 090 393756 (L.M.S.), (+)39 0971 202223 (A.R.).

(1) (a) Schubert, H. L.; Raux, E.; Wilson, K. S.; Warren, M. J. *Biochemistry* **1999**, *38*, 10660–10669. (b) Wu, C.-K.; Dailey, H. A.; Rose, J. P.; Burden, A.; Sellers, V. M.; Wang, B.-C. *Nat. Struct. Mol. Biol.* **2001**, *8*, 156–160. (c) Walker, C. J.; Willows, R. D. *Biochem. J.* **1997**, *327*, 321–333.

(2) Adler, A. D.; Longo, F. R.; Kampas, F.; Kim, J. *J. Inorg. Nucl. Chem.* **1970**, *32*, 2443–2445.

(3) Fleischer, E. B.; Wang, J. H. *J. Am. Chem. Soc.* **1960**, *82*, 3498–3502.

Published on Web 08/03/2009

groups. Some years later Fleischer et al. reported the detection of a series of SAT complexes in their kinetic investigations of the metalation of tetra(4-pyridyl)porphyrin (TpyP) *in aqueous medium*.[4] In the earlier 70s a series of criticisms were addressed to this initial hypothesis. Burnham and Zuckerman[5] proposed that the putative SAT complex was instead an ion pair between the diacid PPIX porphyrin derivative and a complex anion of the solvated metal. Pasternack et al.[6] interpreted the observed spectral changes described for aqueous solutions on the addition of a metal salt, in terms of the influence of the ionic strength on the protonation equilibria of the porphyrin core. Following this study, Hambright et al.[7] reconsidered their previous observations, that had been misinterpreted as evidence for the postulated SAT intermediate, and pointed to the occurrence of an unusual anion term in the rate law for the insertion of Cu^{2+} ions into a water-soluble tetra-cationic porphyrin. In a subsequent kinetic study, the SAT model has been involved for describing the transition-state complex rather than a pre-equilibrium structure.[8]

Some evidence for a SAT intermediate has been successively reported by Macquet and Theophanides[9] for the Pt(II) insertion in hematoporphyrin IX (HPH_2) under acidic conditions. The suggested mechanism involved (i) the formation of an ion-paired intermediate between the protonated HPH_4^{2+} and $PtCl_4^{2-}$; (ii) the expulsion of two HCl equivalents from the core upon heating with the concomitant coordination of the $PtCl_2$ moiety leading to the SAT intermediate; (iii) the eventual elimination of the last two HCl equivalents leading to the final Pt(II)-porphyrin. On the basis of geometrical considerations about the distances between N atoms at the porphyrin core (from X-ray diffraction data on porphine) and on XPS investigations,[10] these authors suggested that two unprotonated N atoms of adjacent pyrrole rings were coordinating the $PtCl_2$ moiety, similarly to what has been recently reported for rhodium complexes of N-confused porphyrins.[11]

A series of spectroscopic and kinetic investigations on N-methyl substituted porphyrins by Lavallee et al.[12] showed the formation of complexes whose absorption features did not depend on the nature of the metal ion nor the solvent, but resembled those of the monoprotonated form of N-substituted porphyrins. The experimental results were interpreted in terms of ion-pair rather than true SAT complex formation.

In the late 70s, complex equilibria involving free base, monoprotonated, diprotonated porphyrin and SAT complexes were proposed for interpreting the absorption spectral changes during the interaction of TpyP with alkali metal ions in aqueous solutions.[13] Eventually, Fleischer and Dixon[14] tried to settle the debate, reporting as definitive evidence for the formation of a SAT complex the interaction of tetraphenylporphyrin (TPP) and the complex $[Rh(CO)_2Cl]_2$ in acetonitrile. The SAT complex was characterized spectroscopically through UV/vis, IR, and NMR techniques, but still an X-ray crystal structure was lacking.

Funahashi and co-workers[15,16] revived the interest in such issues by reporting a spectroscopic characterization of quite stable copper(II) SAT complexes of various porphyrins in acetonitrile. Exploiting NMR and extended X-ray absorption fine structure (EXAFS) techniques, these authors suggested a six-coordinated copper(II) complex with three different Cu−N bond lengths.[16] Experimental data were satisfactorily reproduced by theoretical investigations combined with EXAFS fits, considering SAT complexes that have two cis pyrrolenine N atoms from the porphyrin core and 2−4 solvent molecules coordinated to copper(II).[17] However, the possibility of a mixture of diprotonated porphyrin and Cu(II)-porphyrin to account for these results was not definitively excluded.

The existence of SAT complexes has been also investigated considering the reverse reaction, that is, the protonation of metallo-porphyrins with strong acids. The use of bulky and poorly coordinating carborane anions produced only the metal ion extraction, leading to the diprotonated porphyrin without any evidence for an intermediate species.[18]

Very recently, Gottfried et al.[19] have reported the direct metal insertion into TPP deposited as a monolayer on a metal surface, hypothesizing a mechanism based on a redox process that is different from the usual metal ion insertion in solution. Density functional theory (DFT) calculations for the related gas-phase processes suggest the formation of an initial complex in which the metal atom is coordinated by the intact unreduced porphyrin and that resembles the sitting-atop complex proposed for porphyrin metalation in solution. In two subsequent steps, the pyrrolic hydrogen atoms are transferred to the metal atom forming H_2, which is eventually released.

Following our continuing interest in the protonation and aggregation behavior of porphyrins in organic solvents,[20−22] we have recently shown that bulky, poorly coordinating

(4) Fleischer, E. B.; Choi, E. I.; Hambright, P.; Stone, A. *Inorg. Chem.* **1964**, *3*, 1284–1287.
(5) Burnham, B. F.; Zuckerman, J. J. *J. Am. Chem. Soc.* **1970**, *92*, 1547–1550.
(6) Pasternack, R. F.; Huber, P. R.; Boyd, P.; Engasser, G.; Francesconi, L.; Gibbs, E.; Fasella, P.; Cerio Venturo, G.; Hinds, L. d. *J. Am. Chem. Soc.* **1972**, *94*, 4511–4517.
(7) Baker, H.; Hambright, P.; Wagner, L. *J. Am. Chem. Soc.* **1973**, *95*, 5942–5946.
(8) Pasternack, R. F.; Vogel, G. C.; Skowronek, C. A.; Harris, R. K.; Miller, J. G. *Inorg. Chem.* **1981**, *20*, 3763–3765.
(9) Macquet, J. P.; Theophanides, T. *Can. J. Chem.* **1973**, *51*, 219–226.
(10) Macquet, J. P.; Millard, M. M.; Theophanides, T. *J. Am. Chem. Soc.* **1978**, *100*, 4741–4746.
(11) Srinivasan, A.; Toganoh, M.; Niino, T.; Osuka, A.; Furuta, H. *Inorg. Chem.* **2008**, *47*, 11305–11313.
(12) (a) Bain-Ackerman, M. J.; Lavallee, D. K. *Inorg. Chem.* **1979**, *18*, 3358–3364. (b) Lavallee, D. K. *Bioinorg. Chem.* **1976**, *6*, 219–227. (c) Lavallee, D. K. *Coord. Chem. Rev.* **1985**, *61*, 55. (d) Lavallee, D. K.; Bain-Ackerman, M. J. *Bioinorg. Chem.* **1978**, *9*, 311–321.
(13) Rau, W. G.; Longo, F. R. *Inorg. Chem.* **1977**, *16*, 1372–1376.
(14) Fleischer, E. B.; Dixon, F. *Bioinorg. Chem.* **1977**, *7*, 129–139.
(15) (a) Inada, Y.; Nakano, Y.; Inamo, M.; Nomura, M.; Funahashi, S. *Inorg. Chem.* **2000**, *39*, 4793–4801. (b) Inada, Y.; Sugimoto, Y.; Nakano, Y.; Funahashi, S. *Chem. Lett.* **1996**, 881–882.
(16) (a) Inada, Y.; Sugimoto, Y.; Nakano, Y.; Itoh, Y.; Funahashi, S. *Inorg. Chem.* **1998**, *37*, 5519–5526. (b) Inamo, M.; Kamiya, N.; Inada, Y.; Nomura, M.; Funahashi, S. *Inorg. Chem.* **2001**, *40*, 5636–5644.
(17) (a) Hsiao, Y.-W.; Ryde, U. *Inorg. Chim. Acta* **2006**, *359*, 1081–1092. (b) Shen, Y.; Ryde, U. *J. Inorg. Biochem.* **2004**, *98*, 878–895.
(18) Gárate-Morales, J. L.; Tham, F. S.; Reed, C. A. *Inorg. Chem.* **2007**, *46*, 1514–1516.
(19) (a) Gottfried, J. M.; Flechtner, K.; Kretschmann, A.; Lukasczyk, T.; Steinruck, H. P. *J. Am. Chem. Soc.* **2006**, *128*, 5644–5645. (b) Shubina, T. E.; Marbach, H.; Flechtner, K.; Kretschmann, A.; Jux, N.; Buchner, F.; Steinruck, H. P.; Clark, T.; Gottfried, J. M. *J. Am. Chem. Soc.* **2007**, *129*, 9476–9483.
(20) (a) De Luca, G.; Romeo, A.; Scolaro, L. M. *J. Phys. Chem. B* **2005**, *109*, 7149–7158. (b) De Luca, G.; Romeo, A.; Scolaro, L. M. *J. Phys. Chem. B* **2006**, *110*, 7309–7315.
(21) De Luca, G.; Romeo, A.; Scolaro, L. M. *J. Phys. Chem. B* **2006**, *110*, 14135–14141.
(22) Rosa, A.; Ricciardi, G.; Baerends, E. J.; Romeo, A.; Scolaro, L. M. *J. Phys. Chem. A* **2003**, *107*, 11468–11482.

Scheme 1. Molecular Structures of the Species under Investigation

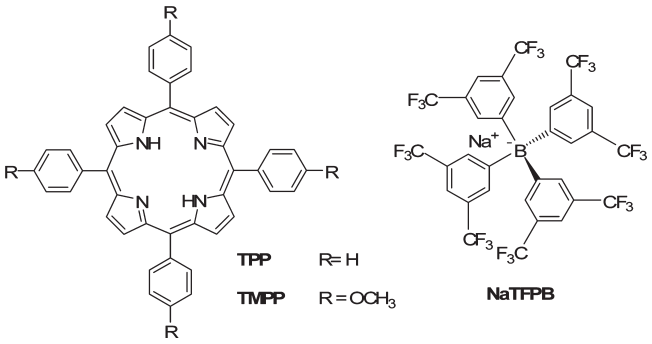

anions, such as tetrakis[3,5-bis(trifluoromethyl)phenyl]borate (TFPB), are efficient in stabilizing the monoprotonated form of tetraphenylporphyrin.[23] DFT and Time Dependent DFT (TDDFT) calculations have provided a rationale for the structural and electronic properties of such species, revealing also the importance of the rotation of the peripheral aryl groups, which parallels synergistically the saddling motion of the porphyrin core in the overall mechanism of protonation in tetra-arylporphyrins.[22,24] Here we report on the formation of SAT complexes of TPP and tetrakis(4-methoxyphenyl)-porphyrin (TMPP) with the sodium salt of TFPB (Scheme 1) in dichloromethane solutions. These complexes have been characterized through a combination of UV/vis absorption, FT-IR, ^{1}H NMR spectroscopy, static and time-resolved emission fluorescence, and DFT/TDDFT analysis of their ground and excited state properties.

Experimental Section

Chemicals. Dicyclohexhyl-18-crown-6 and 1,8-bis(dimethyl-amino)naphthalene (Proton Sponge; PS) were purchased from Aldrich Chemical Co. and used as received. Tetraphenylporphyrin (TPP), tetra(4-nitrophenyl)porphyrin (TNPP), sodium tetrakis[3,5-bis(trifluoromethyl)phenyl]borate, and the corresponding acid (NaTFPB and HTFPB, respectively) were prepared according to literature procedures.[25] Tetra(4-methoxyphenyl)-porphyrin (TMPP) was purchased from Aldrich Chemical Co. and recrystallized from a dichloromethane/diethyl ether mixture.

Spectrophotometric grade and deuterated solvents were distilled under nitrogen from appropriate drying agents[26] and stored over activated 4 Å molecular sieves. In particular: spectrophotometric grade dichloromethane (Sigma) from BaO, after preliminary filtration on activated alumina; chloroform-*d* (D, 99.96% Cambridge Isotope Laboratories) from activated magnesium sulfate and sodium carbonate, after standing for several days over CaH_2. The stock solutions used during the experiments were prepared in freshly purified solvents, stored in the dark and used within a day of preparation. The concentrations of these solutions were determined spectrophotometrically using the molar extinction coefficients at the absorbance maxima (NaTFPB: (4570 ± 30) M^{-1} cm^{-1}, $\lambda = 270$ nm; and Table 1 of the main text).

No relevant differences were observed if the experiments were carried out after drying the solids by standing for many hours under vacuum over P_2O_5 and preparing the solutions in a glovebox, or by using reagents and solvents under atmospheric conditions.

Spectroscopic Methods. UV/vis absorption spectra were measured on a Jasco model V-560 double beam spectrophotometer, using 1 cm cells.

The stoichiometry of the sitting-atop complex has been determined through Job's continuous variation experiments,[27] where solutions of varying porphyrin/NaTFPB molar ratios were prepared while keeping the total molarity of porphyrin and salt constant. Under these conditions, the stoichiometry of the complex is obtained from the abscissa at the maximum in the Job's plot, whose (χ_i ; Y_i) values are given by eqs 1 and 2:[28]

$$\chi_i = [\mathrm{TArP}]_i/([\mathrm{TArP}]_i + [\mathrm{NaTFPB}]_i) \quad (1)$$

$$Y_i = \mathrm{Abs}_{i,\lambda} - \varepsilon_\lambda(\mathrm{TArP})\cdot[\mathrm{TArP}]_i - \varepsilon_\lambda(\mathrm{NaTFPB})\cdot[\mathrm{NaTFPB}]_i \quad (2)$$

Given the experimental results, a simple binding model involving a 1:1 stoichiometric ratio of components was used to determine the binding constants through UV/vis absorption titrations. These were performed by adding known aliquots of a NaTFPB solution into the quartz cell containing a given volume of a porphyrin solution, by means of Hamilton syringes. The UV/vis spectra recorded during the titrations were corrected for dilution. Micromath Scientist 2.0 was used for the least mean square fitting procedure.

Fluorescence (emission and excitation) spectra were recorded on a Jasco model FP-750 spectrofluorimeter equipped with a Hamamatsu R928 photomultiplier, and were not corrected for absorption of the samples. Fluorescence emission was filtered with a high-pass filter (cutoff: 600 nm) to remove excitation overtones. An UV filter (Hoya glass type UV-34, cutoff: 340 nm) was used where necessary to cut off the UV component of the instruments light sources, avoiding the formation of HCl by photodecomposition of dichloromethane.[29] Fluorescence quantum yields have been calculated with respect to TPP in non degassed benzene ($\Phi = 0.11$).[30] Time-resolved experiments have been performed on a homemade apparatus and calculated as described elsewhere.[23] 3D fluorescence experiments were carried out by means of the apposite Jasco software module, which performs an excitation of the sample at different wavelengths in a given range (*excitation scan range*), automatically recording the corresponding emission spectrum (in the *emission scan range*). The *data pitch* defines the scan resolution of emission and excitation ranges. For those emission spectra excited at wavelengths falling into the emission scan range, *λ limiter* sets the minimum distance between the excitation wavelength and the beginning of the emission scan range, to avoid the PMT to be saturated by reflections.

Resonance light-scattering (RLS) experiments were performed on the above-mentioned spectrofluorometer, adopting a synchronous scan protocol with a right angle geometry.[31] No correction has been applied for absorbance of the samples.

(23) De Luca, G.; Romeo, A.; Scolaro, L. M.; Ricciardi, G.; Rosa, A. *Inorg. Chem.* **2007**, *46*, 5979–5988.
(24) Rosa, A.; Ricciardi, G.; Baerends, E. J. *J. Phys. Chem. A* **2006**, *110*, 5180–5190.
(25) (a) Adler, A. D.; Longo, F. R.; Finarelli, J. D.; Goldmacher, J.; Assour, J.; Korsakoff, L. *J. Org. Chem.* **1967**, *32*, 476. (b) Brookhart, M.; Grant, B.; Volpe, A. F. J. *Organometallics* **1992**, *11*, 3920–3922. (c) Bettelheim, A.; White, B. A.; Raybuck, S. A.; Murray, R. W. *Inorg. Chem.* **1987**, *26*, 1009–1017.
(26) (a) Leonard, J.; Lygo, B.; Procter, G. *Advanced practical organic chemistry*, 2nd ed.; Nelson Thornes Ltd.: Cheltenham, U.K., 1995. (b) Weissberger, A.; Proskauer, E. S.; Riddick, J. A.; Toops, E. E. *Techniques of Organic Chemistry*; Interscience Publishers: New York, 1955; Vol. *VII*: Organic Solvents.
(27) Job, P. *Ann. Chim.* (*Paris*) **1928**, *9*, 113–203.
(28) Hirose, K. In *Analytical Methods in Supramolecular Chemistry*; Schalley, C., Ed.; Wiley-VCH Verlag GmbH & Co. KGaA: Weinheim, 2007, pp 17−54.
(29) Scolaro, L. M.; Romeo, A.; Castriciano, M. A.; De Luca, G.; Patanè, S.; Micali, N. *J. Am. Chem. Soc.* **2003**, *125*, 2040–2041.
(30) Seybold, P. G.; Gouterman, M. *J. Mol. Spectrosc.* **1969**, *31*, 1–13.
(31) Pasternack, R. F.; Collings, P. J. *Science* **1995**, *269*, 935–939.

FT-IR spectra were acquired on a Perkin-Elmer spectrometer mod. Spectrum BX as solutions in $CDCl_3$. ^1H NMR spectra were obtained on a Bruker AMX-R 300 spectrometer equipped with a broadband probe operating at 300.13 MHz. Sample solutions in $CDCl_3$ were referenced to the internal residual solvent peak. Chemical shifts (δ) are reported in parts per million downfield from TMS, and coupling constants in hertz.

Quantum Chemical Calculations. The ground state molecular structures of the SAT model complexes, [NaTPP(PF_6)] and [NaTMPP(PF_6)], of the parent free bases and of $NaPF_6$ were fully optimized (without constraints) at the DFT level employing the standard GGA functional Becke88−Perdew86 (BP86).[32] The molecular structure of the S_1 excited state of the SAT complexes was optimized at the TDDFT[33,34] level also employing the BP86 functional. The molecular structures of the ground and excited states were confirmed to be energy minima by calculating the harmonic vibrational frequencies. Solvation effects on the relative stabilities of the ground state optimized structures of the model SAT complexes were evaluated using the conductor-like continuum solvent model (COSMO).[35] Thermodynamic parameters for the formation of the SAT complexes in the gas-phase were computed using the data from the ground state frequency calculations. Basis set superposition error (BSSE) on the binding energy (ΔE) was evaluated following the a posteriori method proposed by Boys and Bernardi.[36] The incidence of BSSE on the binding energies was found to be negligible (5.6 and 6.0 kJ/mol for SAT_{TPP} and SAT_{TMPP}, respectively). The reaction enthalpies under standard conditions (298.15 K and 1 atm) were derived from the BSSE corrected binding energies including the zero-point energy (ZPE) and temperature corrections. The entropic terms for translational, rotational, and vibrational motions were obtained from standard expressions.[37]

Vertical absorption energies and oscillator strengths of the lowest singlet excited states of the SAT complexes and of the parent free bases were computed at TDDFT level using both pure (BP86) and hybrid (B3LYP)[38] functionals. The TDDFT calculations were performed at the DFT/BP86 ground state geometries of the complexes. Vertical emission energies of the S_1 excited state of the SAT complexes were computed at TDDFT/BP86 level using the TDDFT/BP86 optimized geometries of this state.

Ground state equilibrium structures, thermodynamic data, and excited state properties were computed with Turbomole V5−7[39] employing the Karlsruhe triple-ζ valence quality basis sets augmented by one set of polarization functions (TZVP).[40] In the DFT/BP86 calculations, the resolution of the identity (density fitting) approach was used to save computer time.[41] To analyze and quantify the electronic factors governing the formation of the SAT complexes we have used the energy-partitioning scheme implemented in the Amsterdam Density Functional (ADF) program,[42,43] which was originally developed for Hartree−Fock wave functions by Morokuma[44] and modified for the relaxation energy (or orbital interaction term) by Ziegler and Rauk.[45]The energy decomposition is for the bonding between the free base porphyrins (TPP, TMPP) and $NaPF_6$. According to the energy partitioning scheme, the overall bond energy ΔE is made up of two major components (eq 3):

$$\Delta E = \Delta E_{prep} + \Delta E_{int} \quad (3)$$

In this formula, the preparation energy ΔE_{prep} is the energy needed to deform the separate molecular fragments from their equilibrium structure to the geometry that they attain in the overall molecular system. The interaction energy ΔE_{int} is the energy released when the prepared fragments are brought together into the position they have in the overall molecule. It is analyzed for our model systems in the framework of the Kohn−Sham (KS) MO model, using a Morokuma-type decomposition into electrostatic interaction, Pauli repulsion (or exchange repulsion), and (attractive) orbital interactions (eq 4):[43]

$$\Delta E_{int} = \Delta V_{elstat} + \Delta E_{Pauli} + \Delta E_{oi} \quad (4)$$

The term ΔV_{elstat} corresponds to the classical electrostatic interaction between the unperturbed charge distributions of the prepared (i.e., deformed) fragments and is usually attractive. The second term in eq 4, ΔE_{Pauli}, refers to the repulsive interactions between the fragments, which are caused by the fact that two electrons with the same spin cannot occupy the same region in space. ΔE_{Pauli} is calculated by enforcing the KS determinant on the superimposed fragments to obey the Pauli principle by antisymmetrization and renormalization. The ΔE_{Pauli} term comprises the three- and four-electron destabilizing interactions between occupied orbitals and corresponds to the intuitive concept of steric repulsion[46] that is widely used in chemistry. The stabilizing orbital interaction term, ΔE_{oi}, is calculated in the final step of the energy partitioning analysis when the KS orbitals relax to the fully converged ground-state wave function of the total molecule. This term accounts for charge transfer (interaction between occupied orbitals on one molecular fragment and unoccupied orbitals on the other), and polarization (empty/occupied orbital mixing on one fragment).[44] The ADF calculations were performed with the BP86 functional and a TZ2P basis set, which is an uncontracted triple-ζ STO basis set with one 3d and one 4f polarization function for C, N, O, F, and P atoms, one 3p, one 3d, and one 4f for Na, one 2p and one 3d for H.

Results and Discussion

Spectroscopic Studies. (a). Absorption and Fluorescence Spectroscopies. During our recent studies on the presence in solution of monoacid tetraphenylporphyrin (TPP) derivatives,[23] an unexpected color change was detected when sodium tetrakis[3,5-bis(trifluoromethyl)-phenyl]borate (NaTFPB) was added to solutions of this

(32) Becke, A. D. *Phys. Rev. A* **1988**, *38*, 3098–3100. Perdew, J. P.; Yue, W. *Phys. Rev. B* **1986**, *33*, 8800–8802.
(33) (a) Gross, E. U. K.; Dobson, J. F.; Petersilka, M. In *Density Functional Theory*; Nalewajski, R. F., Ed.; Springer: Heidelberg, 1996. (b) Casida, M. E. In *Recent Advances in Density Functional Methods*; Chong, D. P., Ed.; World Scientific: Singapore, 1995; Vol. *1*, p 155. (c) Parr, R. G.; Yang, W. *Density Functional Theory of Atoms and Molecules*; Oxford University Press: New York, 1989.
(34) Dreuw, A.; Head-Gordon, M. *Chem. Rev.* **2005**, *105*, 4009–4037.
(35) (a) Klamt, A.; Schuurmann, G. *J. Chem. Soc., Perkin Trans. 2* **1993**, 799–805. (b) Klamt, A.; Jonas, V. *J. Chem. Phys.* **1996**, *105*, 9972–9981.
(36) Boys, S. F.; Bernardi, F. *Mol. Phys.* **1970**, *19*, 553–566.
(37) McQuarrie, D. A. *Statistical Thermodynamics*; University Science Books: New York, 1973.
(38) (a) Becke, A. D. *J. Chem. Phys.* **1993**, *98*, 5648–5652. (b) Lee, C.; Yang, W.; Parr, R. G. *Phys. Rev. B* **1988**, *37*, 785–789.
(39) Ahlrichs, R.; Bär, M.; Häser, M.; Horn, H.; Kölmel, C. *Chem. Phys. Lett.* **1989**, *162*, 165–169.
(40) Schäfer, A.; Huber, C.; Ahlrichs, R. *J. Chem. Phys.* **1994**, *100*, 5829–5835.
(41) Eichkorn, K.; Treutler, O.; Ohm, H.; Haser, M.; Ahlrichs, R. *Chem. Phys. Lett.* **1995**, *242*, 652–660.
(42) (a) *SCM, ADF2008.01*; Theoretical Chemistry, Vrije Universiteit Amsterdam: The Netherlands, 2008; http://www.scm.com. (b) Baerends, E. J.; Ellis, D. E.; Ros, P. *Chem. Phys.* **1973**, *2*, 41–51. (c) Fonseca Guerra, C.; Snijders, J. G.; te Velde, G.; Baerends, E. J. *Theor. Chem. Acc.* **1998**, *99*, 391–403.
(43) Bickelhaupt, F. M.; Baerends, E. J. *Rev. Comput. Chem.* **2000**, *15*, 1–86.
(44) Morokuma, K. *J. Chem. Phys.* **1971**, *55*, 1236–1244.
(45) Ziegler, T.; Rauk, A. *Theor. Chim. Acta* **1977**, *46*, 1–10.
(46) (a) Fujimoto, H.; Osamura, Y.; Minato, T. *J. Am. Chem. Soc.* **1978**, *100*, 2954–2959. (b) Kitaura, K.; Morokuma, K. *Int. J. Quantum Chem.* **1976**, *10*, 325–340. (c) van den Hoek, P. J.; Kleyn, A. W.; Baerends, E. J. *Comments At. Mol. Phys.* **1989**, *23*, 93–110.

Table 1. UV/vis Absorption, Emission, and Photophysical Parameters of TPP, TMPP, and the Relative SAT Complexes in Dichloromethane at 298 K

species	B band	ε (M^{-1} cm^{-1})	Q bands	emission	Φ_f[a,b]	τ_f/ns (%) [b]
TPP	418	4.78×10^5[c]	515; 549; 592; 646	651; 716	0.10	8.40
NaTPP(TFPB)	424; 440	3.50×10^5[d]	519; 557; 589; 636	665; 706	0.07	1.73 (0.95); 2.85 (0.05)
TMPP	421	4.57×10^5[c]	518; 556; 595; 651	657; 721	0.11	7.57
NaTMPP(TFPB)	445	2.34×10^5	555; 650	685; 718	0.04	1.34 (0.98); 2.90 (0.02)

[a] Relative to TPP in non degassed benzene ($\Phi = 0.11$); ref 30. [b] Non degassed samples. [c] Ref 61. [d] Main feature (424 nm).

porphyrin in CH_2Cl_2. A systematic investigation of this phenomenon has shown that the species present in a TPP solution saturated with NaTFPB possesses clearly distinct UV/vis spectral features with respect to those of neat TPP (Figure 1). The B-band is bathochromically shifted and consists of a major component centered around 424 nm that presents an intense shoulder around 440 nm, and the Q-band pattern is remarkably different from the one usually observed for free base porphyrins (Figure 1a). As shown in Figure 1b, significant changes occur also in the luminescence spectra, with a red shift of the two-banded emission as compared to the starting TPP, accompanied by a decrease of the ratio between the intensity of two features (higher energy band/lower energy band). The emission profile of solutions containing both TPP and NaTFPB is found to be independent of the excitation wavelength (see 3D fluorescence experiments, Figure 2 and Supporting Information, Figure S2), pointing to the presence of an isolated fluorophore. In agreement with this conclusion all excitation spectra match the corresponding absorption profile, regardless of the emission wavelength chosen for the observation (Figure 1c, 2 and Supporting Information, Figure S2). As for TPP, time-resolved fluorescence experiments show that in the presence of NaTFPB the emission decay is mainly dominated by a monoexponential component (a second component accounts for only 5% of the total change, see Table 1), but in this case a substantial shortening of the measured lifetime is displayed as compared to that of the free base.

Since the formation of metallo-porphyrins coordinating alkali metal ions had been previously reported both in aqueous and organic phases,[19,47−49] at first we considered a common metalation reaction of the porphyrin macrocycle as a plausible explanation of the observed spectroscopic evidence. However, a strong base or a reducing agent had been used in those cases to remove the hydrogen atoms of the porphyrin core and to lead to the porphyrinato species. Under our experimental conditions, the formation of the meso-tetraphenylporphyrinato-disodium(I) derivative (Na_2TPP) can be ruled out on spectroscopic evidence. In fact, as previously reported in the literature and in contrast with our findings, Na_2TPP displays an absorption spectrum with a sharp B-band accompanied by two Q-bands at longer wavelengths,[49] a profile which is commonly observed for other tetra-aryl substituted metallo-porphyrins. Moreover, in our study, the fluorescence emission and excitation profiles of the

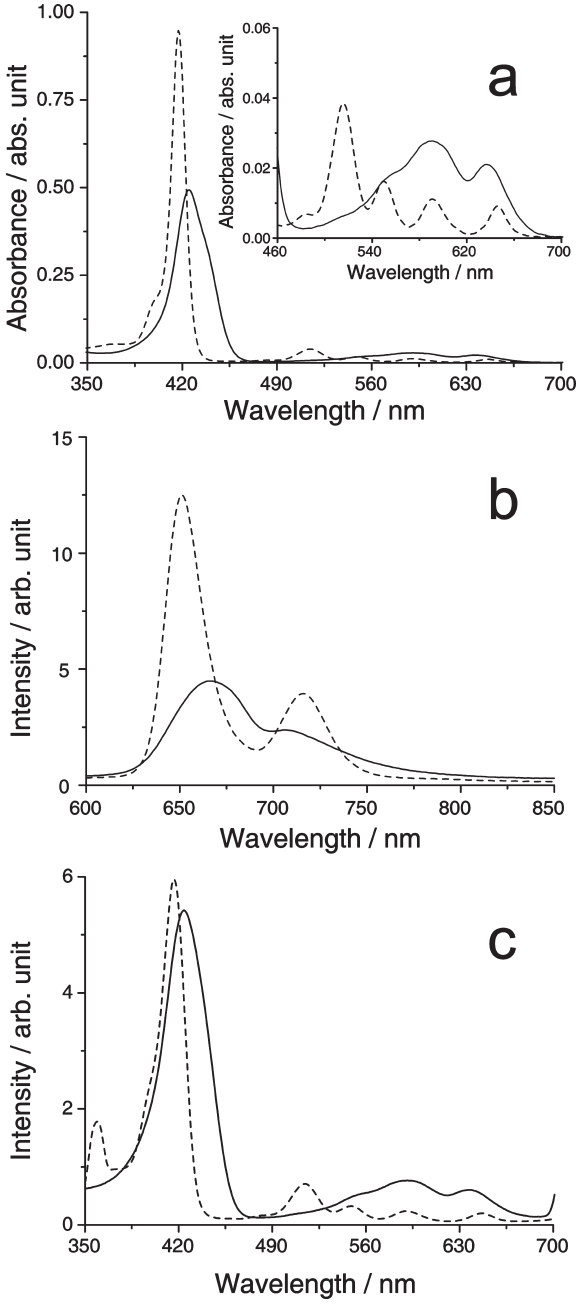

Figure 1. Absorption (a), fluorescence emission (b), and excitation (c) spectra of [NaTPP(TFPB)] SAT complex (solid lines). The optical properties of TPP (dashed lines) are reported for comparison. (a, inset) Q-band region. (b) Excitation wavelengths: TPP = 387 nm; SAT = 397 nm; abs(λ_{exc}) = 0.11 abs. unit. (c) Emission wavelengths: TPP = 716 nm; SAT = 709 nm. [TPP] = 2.1×10^{-6} M; [NaTFPB] = saturated solution.

(47) (a) Allison, J. B.; Becker, R. S. *J. Phys. Chem.* **1963**, *67*, 2675–2679. (b) Brand, H.; Capriotti, J. A.; Arnold, J. *Inorg. Chem.* **1994**, *33*, 4334–4337. (c) Islam, M. Q.; Hambright, P. *Transition Met. Chem.* **1998**, *23*, 727–733. (d) Richards, R. A.; Hammons, K.; Joe, M.; Miskelly, G. M. *Inorg. Chem.* **1996**, *35*, 1940–1944.

(48) Arnold, J.; Dawson, D. Y.; Hoffman, C. G. *J. Am. Chem. Soc.* **1993**, *115*, 2707–2713.

(49) (a) Dorough, G. D.; Miller, J. R.; Huennekens, F. M. *J. Am. Chem. Soc.* **1951**, *73*, 4315–4320. (b) Lee, C. Y.; Levin, G. *J. Phys. Chem.* **1979**, *83*, 3165–3168.

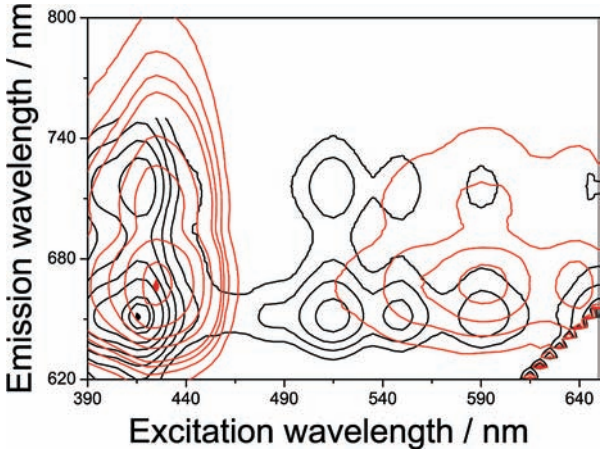

Figure 2. Contour plots of the 3D fluorescence experiments (see Supporting Information, Experimental Section) carried out on TPP (black lines) and [NaTPP(TFPB)] SAT complex (red lines), showing the completely different emission properties of the two species. The level curves represent points on the 3D surface having same fluorescence intensity, as a function of both excitation and emission wavelengths. Normalization of the intensity values has been rendered by plotting nine level curves for each species (four of them describing the Q-bands region), the small filled areas at the bottom-left corner indicating the highest emission intensity.

species obtained at the highest Na^+/TPP ratio attainable (saturated NaTFPB solution in CH_2Cl_2 containing a very low porphyrin concentration, [TPP] = 10^{-8} M) always corresponded to those shown in Figure 1, which have been regarded as characteristic of the end point of the reaction.

A remarkable similarity can be noticed on comparing the optical properties of the solution containing both TPP and NaTFPB to those of the monoprotonated TPP derivative in the presence of the $TFPB^-$ anion (Figure 3a and Supporting Information, Figure S3).[23] This likeness prompted us to verify the absence of any acid contamination of CH_2Cl_2, even though the solvent had been extensively purified before use in these experiments. To this end, when a Proton Sponge (PS) is added to the chlorinated solvent, the spectral features displayed by this solution correspond to those of unprotonated PS. Furthermore, acid contamination of NaTFPB has been excluded since, once the absorption profile of the TPP solution is that shown in Figure 3a (solid line), it does not change on increasing salt concentration: if acid impurities were present in NaTFPB, adding more salt should result in a further porphyrin protonation.[50] Moreover, our recent studies on porphyrin acid derivatives in organic solvents demonstrated that proton transfer to these molecules involves equilibria between ion pairs, and an excess of NaTFPB shifts the equilibria toward the diacid species.[20−23] Hence, in a low polarity and aprotic solvent such as CH_2Cl_2 the equilibria between TPP free base and its mono- or diacid derivatives should not be observed unless acid is deliberately added, circumventing the complicating occurrence of multiple equilibria experienced in water.[13] After having ruled out acid contamination of the

(50) When traces of acid are added to a solution containing both TPP and NaTFPB, the absorption profile of the resulting solution becomes much different to that shown by the SAT complex (see Supporting Information, Figure S1), leading to eventual formation of the diacid TPP in the TFPB form.

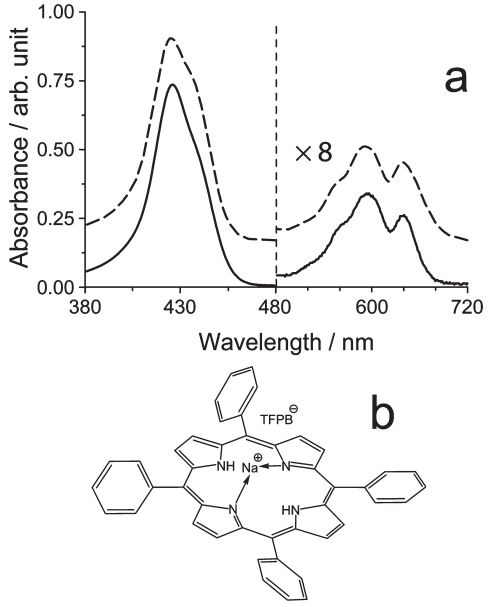

Figure 3. (a) Comparison between the UV/vis absorption profiles of [NaTPP(TFPB)] and [HTPP(TFPB)] CH_2Cl_2 solutions (solid and dashed lines, respectively). (b) Hypothesized structure of the Na^+ sitting-atop complex of TPP.

solutions, the aforementioned analogy with the optical properties of TPP monoacids suggested to us that, in the low polarity environment provided by CH_2Cl_2, the sodium cation might behave much like the hydrogen ion. This picture is further supported by literature studies on the complexation of alkali metal ions by pyridine or THF in aprotic solvents.[51] Hence, the poorly solvated Na^+ could be coordinated by the two lone pairs of the pyrrolenine nitrogen atoms at the porphyrin core without the simultaneous expulsion of the two pyrrole hydrogen atoms (Figure 3b), that is, leading to a *sitting-atop* complex ([NaTPP(TFPB)], SAT).[3] As previously discussed, these species have been often proposed as intermediates in the mechanism of porphyrins metalation, and their actual existence has been demonstrated only in low polarity solvents.[3−5,7,13−16,52]

The formation of a SAT complex has been attempted also with tetra(4-nitrophenyl)porphyrin (TNPP) and tetra(4-methoxyphenyl)porphyrin (TMPP), which represent a weaker and stronger base, respectively, than TPP.[53] The general behavior of the three chromophores is very similar. The limited solubility in CH_2Cl_2 of both TNPP and NaTFPB does not allow for the same thorough investigation carried out on TPP, but a first very interesting remark can be made: on increasing TNPP concentration in saturated NaTFPB solutions the porphyrin spectral features become similar to those exhibited by TPP under the same experimental conditions, and that

(51) (a) Perelygin, I. S.; Shatokhin, S. A. *J. Mol. Struct.* **1998**, *440*, 89–96. (b) Ahmad, N.; Day, M. C. *J. Inorg. Nucl. Chem.* **1978**, *40*, 1383–1385. (c) Greenberg, M. S.; Popov, A. I. *Spectrochim. Acta, A* **1975**, *A31*, 697–705. (d) Greenberg, M. S.; Bodner, R. L.; Popov, A. I. *J. Phys. Chem.* **1973**, *77*, 2449–2454.

(52) (a) Letts, K.; Mackay, R. A. *Inorg. Chem.* **1975**, *14*, 2993–2998. (b) Inamo, M.; Kohagura, T.; Kaljurand, I.; Leito, I. *Inorg. Chim. Acta* **2002**, *340*, 87–96.

(53) (a) Meot-Ner, M.; Adler, A. D. *J. Am. Chem. Soc.* **1975**, *97*, 5107–5111. (b) Gündüz, N.; Gündüz, T.; Hayvali, M. *Talanta* **1999**, *48*, 71–79.

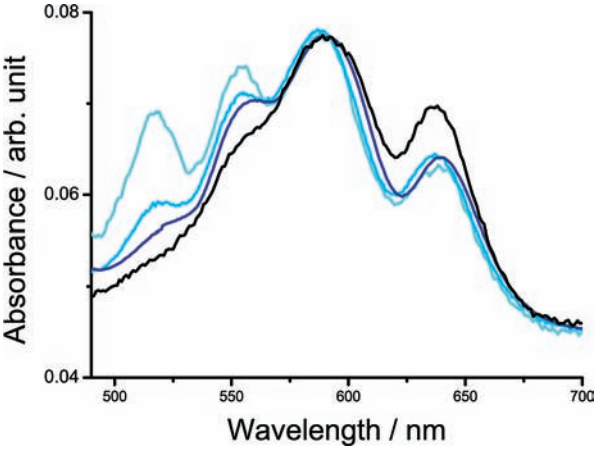

Figure 4. Absorption spectra (Q-bands region) of NaTFPB saturated solutions in CH_2Cl_2 containing increasing concentration of TNPP (going from light cyan to blue) compared to the spectrum of TPP (black) recorded under the same experimental conditions. On considering the trend of the spectral change concerning TNPP, the black curve can be regarded as the limiting spectrum for its SAT complex.

have been attributed to SAT (Figure 4), even though a complete conversion is not attained because of TNPP precipitation.

The absorption characteristics of the solution containing the SAT complex of TMPP [NaTMPP(TFPB)] display a red-shifted and broad B-band together with an unresolved Q-bands convolution at longer wavelengths (Figure 5a and Table 1). The presence of lone pairs on the oxygen atoms of the methoxyphenyl groups at the *meso* position could be responsible for such unusual absorption profile, giving to TMPP an hyperporphyrin character.[21,54] As shown by Figure 5b, also the emission spectrum is deeply affected by the presence of the sodium salt, with a 30 nm red shift of the high energy band as compared to the free base, and its profile does not depend on the excitation wavelength suggesting the existence of an isolated fluorophore in solution. Accordingly, all excitation profiles recorded at various emission wavelengths agree with the absorption spectrum (inset of Figure 5a, Figure 6, and Supporting Information, Figure S5). As observed for TPP, the decay of TMPP fluorescence emission in the presence of NaTFPB is faster than that of the neat free base (Table 1).

The presence of aggregates has been ruled out on spectroscopic evidence for both TPP and TMPP SAT complexes: (i) Beer's experiments (Figure 7a) have shown a linear dependence of absorbance on porphyrin concentration in saturated NaTFPB solutions, and (ii) RLS profiles (Figure 7b) display wells because of photon loss at absorption maxima consistent with the presence of monomeric species in solution. The stoichiometric ratio between porphyrin and metal cation in the SAT complexes has been determined by the continuous variation method.[27] Figure 8a shows the Job's plot for TPP and TMPP, in which the function Y (see Experimental Section) is plotted against the molar fraction of the free base. The

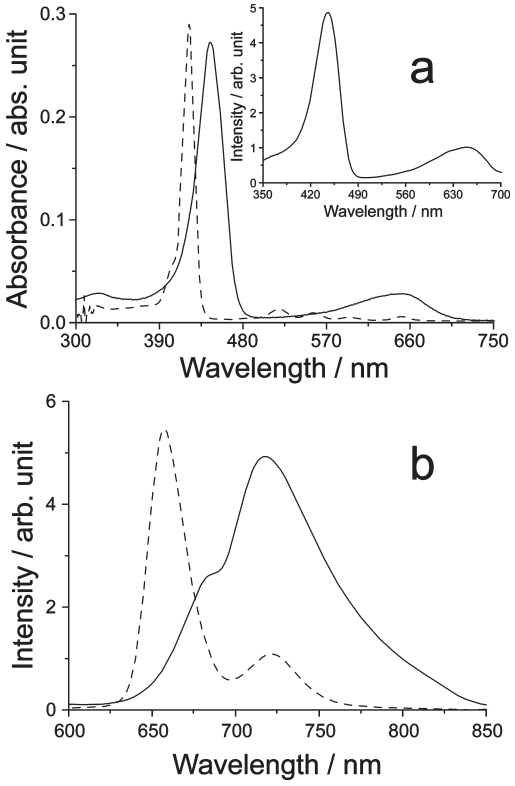

Figure 5. Absorption (a), fluorescence emission (b) and excitation (a, inset) spectra of [NaTMPP(TFPB)] SAT complex (solid lines). Absorption and emission of TMPP are reported for comparison (dashed lines; absorption has been scaled by a factor of 2). (a, inset) Emission wavelength: SAT = 718 nm. (b) Excitation wavelengths: TMPP = 435 nm (intensity scaled by a factor of 4); SAT = 465 nm; abs(λ_{exc}) = 0.10 abs. unit. [TMPP] = 1.3×10^{-6} M; [NaTFPB] = saturated solution.

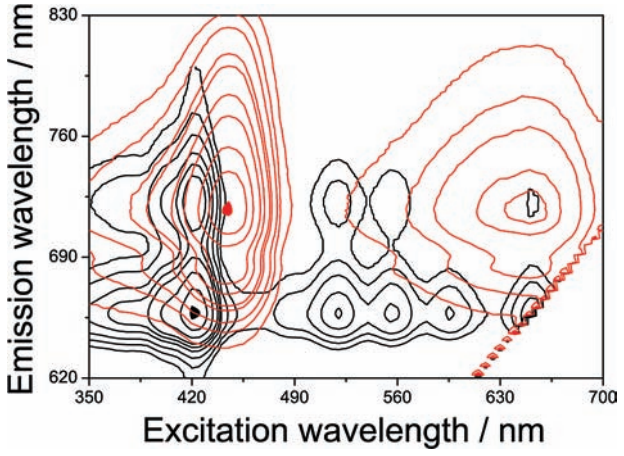

Figure 6. Contour plots of the 3D fluorescence experiments (see Experimental Section) carried out on TMPP (black lines) and [NaTMPP-(TFPB)] SAT complex (red lines), showing the completely different emission properties of the two species. The level curves represent points on the 3D surface having same fluorescence intensity, as a function of excitation and emission wavelengths. Normalization of the intensity values has been rendered by plotting 10 level curves for each species (5 of them describing the Q-bands region), the small filled areas at the bottom-left corner indicating the highest emission intensity.

maximum observed at $\chi_{TMPP} = 0.5$ clearly indicates a 1:1 stoichiometry.

Qualitatively, it has been observed that the porphyrin to NaTFPB ratio needed to completely form the corresponding SAT complex decreases following the trend

(54) (a) Gouterman, M. In *The porphyrins*; Dolphin, D., Ed.; Academic Press: New York, 1978; Vol. *3*, pp 1−165. (b) Hanson, L. K.; Eaton, W. A.; Sligar, S. G.; Gunsalus, I. C.; Gouterman, M.; Connell, C. R. *J. Am. Chem. Soc.* **1976**, *98*, 2672–2674.

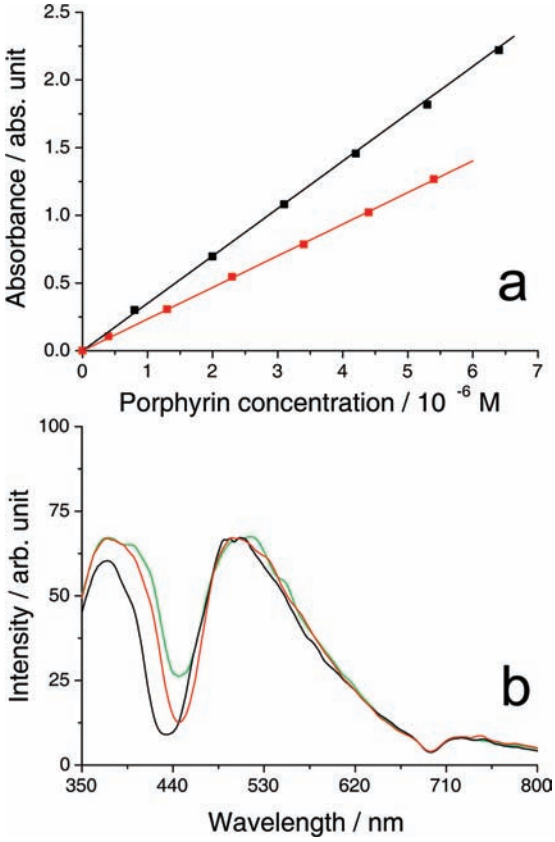

Figure 7. (a) Absorbance measured at absorption maxima vs porphyrin concentration for CH_2Cl_2 solutions of TPP (black) and TMPP (red) SAT complexes. Extinction coefficients, determined through least mean squares fitting of the experimental data, amount $(3.50 \pm 0.03) \times 10^5$ M^{-1} cm^{-1} for TPP ($\lambda_{max} = 424$ nm; $R = 0.9997$), and $(2.34 \pm 0.01) \times 10^5$ M^{-1} cm^{-1} for TMPP ($\lambda_{max} = 445$ nm, $R = 0.9999$). All solutions were saturated in NaTFPB. (b) Resonance light scattering (RLS) experiments carried out on CH_2Cl_2 solutions of TPP (black) and TMPP (red) SAT complexes, at a comparison to that of a NaTFPB saturated solution (green). Experimental conditions: [porphyrin] ~ 4 μM; NaTFPB saturated solution.

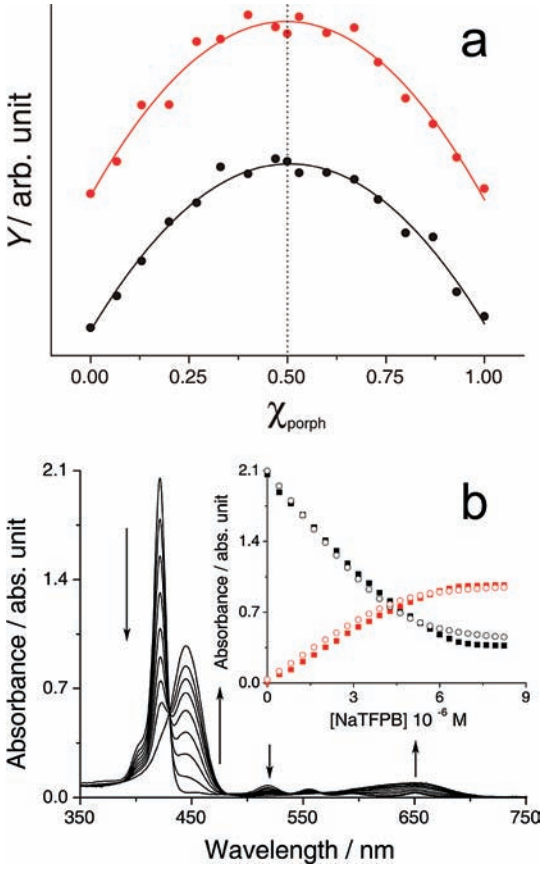

Figure 8. (a) Job's continuous variation experiment to determine the stoichiometry of TPP and TMPP SAT complexes (black and red, respectively): molar fraction of TPP and TMPP is varied while keeping the total concentration of the dye and NaTFPB constant. Dots correspond to absorbance differences (Y function, see Experimental Section) at fixed wavelength for various porphyrin molar fractions. (b) Absorption spectral change upon titration of a TMPP solution in CH_2Cl_2 with NaTFPB ([TMPP] $= 4.6 \times 10^{-6}$ M). The arrows mark the increase of NaTFPB concentration. Inset: absorbance at 421 and 445 nm (black and red symbols, respectively), plotted against NaTFPB concentration. Filled squares: experimental values; empty circles: values obtained after the fitting process to calculate the equilibrium constants.

TNPP > TPP > TMPP, in line with the differences in basicity of the three chromophores.[53] The UV/vis spectroscopic titrations of TMPP and TPP solutions with NaTFPB display several isosbestic points (Figure 8b and Supporting Information, Figure S8, respectively) and they have provided a good estimate[55] of the equilibrium constant for SAT formation, according to the following equation:

$$TArP + \{(Na^+)\cdot(TFPB^-)\} \overset{K_{eq}}{\rightleftarrows} \{(NaTArP^+)\cdot(TFPB^-)\} \quad (5)$$

An estimate of the values of K_{eq} obtained by fitting the absorption titration data follows the basicity trend of the two species, giving $(9 \pm 4) \times 10^5$ L mol^{-1} in the case of TPP and $(5 \pm 2) \times 10^6$ L mol^{-1} for TMPP, respectively.

(b). Infrared and NMR Spectroscopy. On considering the larger binding constant of TMPP with respect to TPP toward NaTFPB, we decided to limit our investigation to the first species. The IR spectra of [NaTMPP(TFPB)] SAT complex, the parent porphyrin, and NaTFPB have been investigated in $CDCl_3$ solution (Figure 9a), the main differences being observed in the high wavenumber region (> 3000 cm^{-1}). As expected, the IR spectrum of TMPP shows a rather sharp peak centered at 3322 cm^{-1} attributable to the N−H stretching, whereas no signal is detectable in the same region in the case of NaTFPB saturated solution. Differently, a 1:1 mixture of TMPP and NaTFPB reveals an equilibrium between the free base and the SAT complex, with the sharp peak of TMPP N−H stretching being accompanied by a new broadband at 3367 cm^{-1}, which can be assigned to the N−H stretching of the SAT complex.

The ^{1}H NMR spectrum of TMPP in $CDCl_3$ displays a series of well resolved peaks: (i) a singlet at δ 8.85 relative to the pyrrole H_β, (ii) two doublets at δ 8.11 and 7.27, attributable to the $H_{3,5}$ and $H_{2,6}$ of the meso aryl substituent groups, (iii) a singlet at δ 4.08 due to the methoxy protons, and (iv) a broad singlet at δ −2.75 relative to the N−H protons. A saturated NaTFPB solution evidences two peaks at δ 7.68 and 7.54 assigned to the $H_{2,6}$ and H_4,

(55) The evaporation of CH_2Cl_2 leads to a certain error on the concentration of the various species which is not quantifiable.

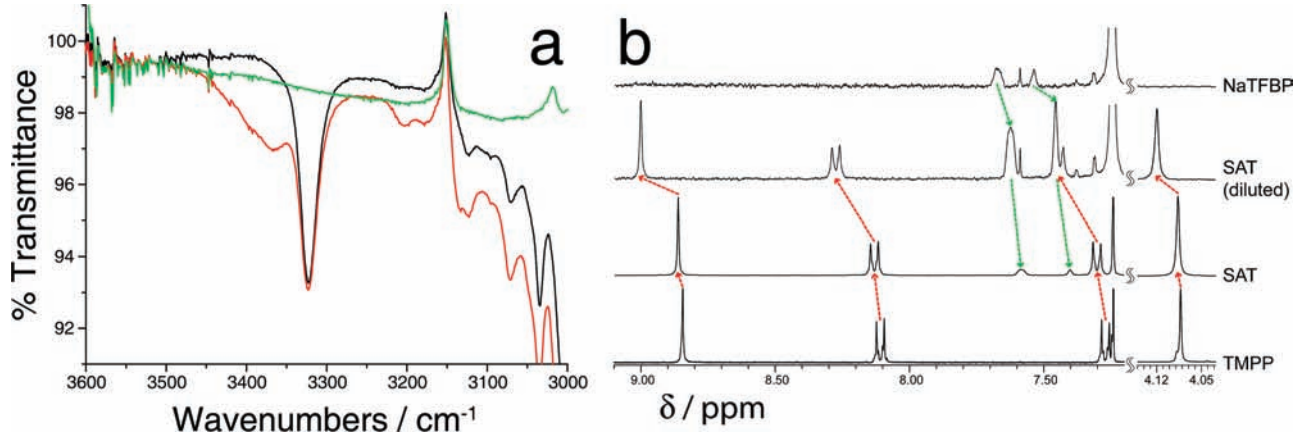

Figure 9. (a) FTIR spectra of $CDCl_3$ solutions of TMPP (black), TMPP SAT/TMPP mixture (red, 5 mg TMPP in 0.7 mL saturated NaTFPB), and saturated NaTFPB (green). (b) ^{1}H NMR spectra of TMPP, NaTFPB, and TMPP SAT (in saturated NaTFPB) at different concentration in $CDCl_3$.

respectively. The addition of TMPP to this saturated solution leads to the disappearance of the NH resonance, probably because of fast exchange on the NMR time scale. All the resonances of the TMPP/NaTFPB mixture are concentration dependent, reflecting the presence of a fast equilibrium between two exchanging species, that is, the free porphyrin and the [NaTMPP(TFPB)] SAT complex. Its limiting chemical shift values are estimated from the most diluted porphyrin solution for the TMPP moiety and from the most concentrated one in the case of TFPB anion. Furthermore, the NaTFPB peaks move to lower frequencies ($\Delta\delta = -0.09$ and -0.14 for $H_{2,6}$ and H_4, respectively), while the porphyrin resonances are affected in the opposite way ($\Delta\delta = +0.15$, $+0.16$, $+0.27$ and $+0.04$ for H_β, $H_{3,5}$, $H_{2,6}$ and $O-CH_3$, respectively). It is worth noticing that the protons of the *meso* phenyl ring are the most downfield shifted, and in particular the ortho protons, which should experience the influence of the bound sodium cation. These experimental findings suggest also the TFPB anion being located on top of the porphyrin plane (in analogy to the theoretical model predicted for $NaPF_6$, vide infra), experiencing the ring current of the aromatic macrocycle.

Theoretical Studies. To further characterize the SAT complexes formed upon titration of TPP and TMPP with NaTFPB, their structural, electronic, and optical properties were theoretically investigated using as models [NaTPP(PF_6)] and [NaTMPP(PF_6)] (hereafter referred to as SAT_{TPP} and SAT_{TMPP}), in which the bulky $TFPB^-$ is replaced by the less encumbering PF_6^-. The use of the PF_6^- in place of $TFPB^-$ has the advantage to render the calculations more tractable while assuring a reasonable modeling of the coordination properties of $TFPB^-$.[23]

(a). Molecular Structures. Two structures were theoretically explored for SAT_{TPP} and SAT_{TMPP}: ***A*** having the sodium ion residing above the tetrapyrrolic cavity and capped by PF_6^-; ***B*** with the sodium ion residing above the tetrapyrrolic cavity and PF_6^- pointing to the cofacial pair of trans pyrrole NH groups on the opposite face of the macrocycle. ***A*** is compatible with the assumption that the sodium salt is mainly present in CH_2Cl_2 solution in the form of neutral ion pair, which is quite realistic in view of the low-polarity and weakly coordinating capability of this solvent. ***B*** takes into account the presence of the sodium salt in the dissociated ionic form, which cannot be excluded a priori. For the TMPP macrocycle, an *udud* (*u* = up, *d* = down) orientation of the peripheral methoxy groups was assumed. Unconstrained geometry optimization of ***A*** and ***B*** in the gas-phase revealed that the latter is by far less stable than the former, the energy difference amounting to 59.6 and 57.4 kJ/mol for SAT_{TPP} and SAT_{TMPP}, respectively. The relative stability of ***A*** and ***B*** does not change significantly upon inclusion of solvent effects. Indeed, calculation of the solvation energies (single-point) using COSMO showed ***A*** being still significantly more stable than ***B*** (44.0 and 42.1 kJ/mol for SAT_{TPP} and SAT_{TMPP}, respectively). As ***B*** is energetically very unfavorable for both complexes, ground- and excited-state theoretical studies have been restricted to the most stable ***A*** structure. The C_1 symmetry optimized structures of SAT_{TPP} and SAT_{TMPP} are displayed in Figure 10.

The most relevant structural parameters computed for the model complexes and the parent free bases are gathered in Table 2. In both SAT complexes the sodium ion is bound to the four nitrogen atoms of the porphyrin ring, the bond with the iminic N atoms being 0.16−0.17 Å shorter than that with the pyrrolic nitrogen atoms (cf. Table 2). The involvement of the pyrrolic N atoms in the interaction with the sodium ion leads to a modest but not negligible elongation of the N−H bonds, pyramidalization of the hydrogen atoms, and blue shift of the N−H stretching frequencies. The shifts of 49 cm^{-1} and 58 cm^{-1} calculated for SAT_{TPP} and SAT_{TMPP}, respectively, are in good agreement with the 45 cm^{-1} value determined experimentally for [NaTMPP(TFPB)]. The calculated Na−N(iminic) bond lengths are slightly longer than those found in the crystalline $Na_2(THF)_4OEP$ (OEP = 2,3,7,8,12,13,17,18-octaethylporphyrinato), where each six-coordinate sodium ion is bound to all four N atoms of the porphyrin [Na−N 2.452, 2.508(2) Å],[48] but slightly shorter than those found in $[Na(THF)_3]$[FeTPP], in which the sodium ion is bound to two N atoms of the porphyrin [Na−N 2.784(4), 2.825(4) Å].[56] In SAT_{TPP} and SAT_{TMPP} the sodium ion is also bound to three of the fluorine atoms of the PF_6 anion, giving a seven-coordinated sodium. The calculated Na−F distances (2.365−2.410 Å) compare

(56) Mashiko, T.; Reed, C. A.; Haller, K. J.; Scheidt, W. R. *Inorg. Chem.* **1984**, *23*, 3192–3196.

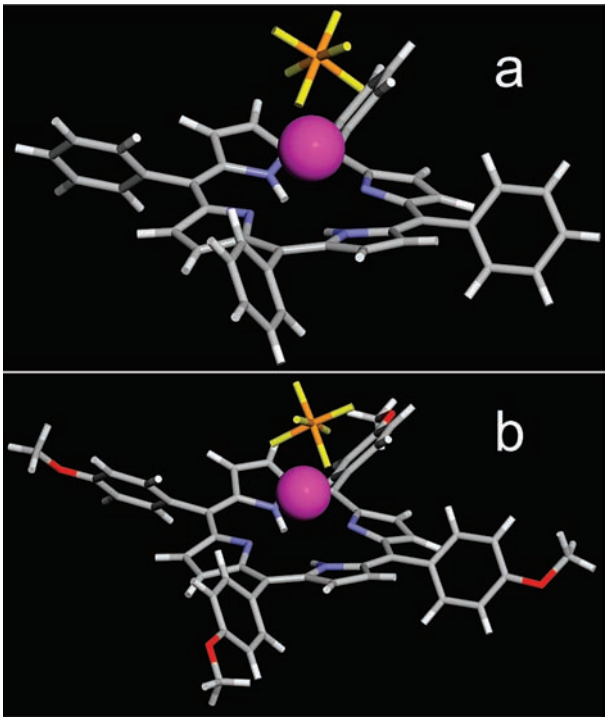

Figure 10. DFT-optimized *A* structures of SAT_{TPP} (a) and SAT_{TMPP} (b).

Table 2. Selected Bond Lengths (Å), Bond Angles (deg), and Metrical Parameters Calculated for SAT_{TPP}, SAT_{TMPP}, and the Corresponding Free Base Porphyrins, TPP and TMPP

	TPP[a]	SAT_{TPP}	TMPP[b]	SAT_{TMPP}
$Na-F_1$		2.357		2.365
$Na-F_2$		2.380		2.396
$Na-F_3$		2.392		2.410
$Na-N^c$		2.837/2.672		2.835/2.662
$C_\alpha-N^c$	1.380/1.373	1.385/1.382	1.381/1.374	1.386/1.381
$C_\alpha-C_\beta{}^c$	1.436/1.460	1.431/1.453	1.436/1.460	1.430/1.452
$C_\beta-C_\beta{}^c$	1.374/1.360	1.377/1.361	1.375/1.360	1.378/1.362
$C_m-C_1{}^d$	1.498	1.492	1.496	1.487
$O-C_4{}^d$			1.372	1.368
$C_\alpha-N-C_\alpha{}^c$	110.5/105.2	110.5/104.9	110.6/105.3	110.6/105.0
$C_\alpha-C_m-C_\alpha{}^d$	125.4	124.8	125.3	124.4
$\varphi^{e,d}$	1.9	13.4	2.5	15.9
$\omega^{f,c}$	8.8/0.0	0.1/0.1	0.0/9.7	1.3/1.3
$\theta^{g,d}$	69.3	52.5	67.2	47.5

[a] Optimized without symmetry constraints from the X-ray triclinic molecular structure; ref 62. [b] Optimized without symmetry constraints from the X-ray molecular structure; ref 63. [c] Average values for pyrrole/pyrrolenine rings. [d] Average values. [e] φ is the $C_\alpha-N-N-C_\alpha$ torsional angle, which provides a measure of the tilting of adjacent pyrrole/pyrrolenine ring planes (saddling). [f] ω is the $C_\alpha-N-N-C_\alpha$ torsional angle of the opposite pyrrole or pyrrolenine ring planes with respect to an axis through the nitrogen atoms (ruffling). [g] θ is the $C_2-C_1-C_m-C_m$ torsional angle, which provides a measure of the tilting of the aryl ring plane with respect to the porphyrin ring plane.

well to those found in the crystal structure of the (15-crown-5)$NaPF_6$ [2.46(2) and 2.40(2) Å][57] and [CpRu(benzo-15-crown-5)($NaPF_6$)]BPh_4 [2.400(4) and 2.334(3) Å][58] complexes, in which the sodium ion also exhibits a seven-coordination, although in this case it is bound to only two fluorine atoms of the PF_6 anion. When comparing the bond parameters of the SAT complexes to those of the parent free bases, it is apparent that the major structural effect of the interaction with $NaPF_6$ is the saddling distortion of the macrocycle. With the only exception of the $C_\alpha-N$(iminic) distance that experiences an appreciable elongation, bond lengths and angles of the porphyrin core are not affected by the interaction with $NaPF_6$. The saddling distortion of the porphyrin core is primarily driven by the necessity to improve the overlap between the acceptor Na-3s orbital and the iminic N lone pairs, and it is larger in SAT_{TMPP} than in SAT_{TPP}. Also, the tilting angle of the *meso*-aryl rings (θ) in SAT_{TMPP} is larger than in SAT_{TPP}, in agreement with experimental data[59] and recent theoretical studies[24] showing that a larger degree of saddling correlates with more acute porphyrin-aryl dihedral angles. In line with the stronger basicity of TMPP as compared to TPP, the larger degree of saddling and slightly shorter Na−N distances calculated for SAT_{TMPP} point to a more effective Na-porphyrin interaction in this complex with respect to SAT_{TPP}.

Table 3. Thermodynamics and Equilibrium Constants for the Formation of SAT_{TPP} and SAT_{TMPP}[a]

	ΔH^b	$-T\Delta S^b$	ΔG^b	K, calcd	K, exp.[c]
SAT_{TPP}	−75.4	43.8	−31.6	3.4×10^5	$(9 \pm 4) \times 10^5$
SAT_{TMPP}	−86.6	51.3	−35.3	1.5×10^6	$(5 \pm 2) \times 10^6$

[a] $T = 298.15$ K, $P = 1$ atm. [b] All values in kJ mol^{-1}. [c] This work.

(b). Formation of SAT_{TPP} and SAT_{TMPP}: Thermodynamic Aspects. The thermodynamic parameters and the equilibrium constants computed for the formation of SAT_{TPP} and SAT_{TMPP} from $NaPF_6$ and the parent porphyrins in the gas-phase are reported in Table 3. As inferred from these data, the computed equilibrium constant values are very close to those spectroscopically determined for [NaTPP(TFPB)] and [NaTMPP(TFPB)]. Such a good agreement between theory and experiment suggests that SAT_{TPP} and SAT_{TMPP} are realistic models for the experimentally identified SAT complexes. Inspection of the thermodynamic data in Table 3 reveals that the formation of SAT_{TMPP} is energetically favored over that of SAT_{TPP}, mainly because of a more negative enthalpic term. This is consistent with the calculated bond parameters pointing to a stronger sodium-porphyrin interaction in the first complex.

(c). Nature and Strength of the Sodium-Porphyrin Interaction. To understand the electronic factors governing the formation of the SAT complexes, we have performed for SAT_{TPP} and SAT_{TMPP} an energy decomposition analysis of the interaction between the pertinent free base porphyrin and $NaPF_6$. The energy decomposition analysis results are given in Table 4.

Comparing the ΔE_{oi} and ΔV_{elstat} terms (see Experimental Section) it is possible to note that the largest stabilizing contribution to the interaction energy (ΔE_{int}) comes from electrostatics, particularly in the SAT_{TMPP} complex, although covalent interactions are an important component of the sodium-porphyrin interaction energy.

(57) Weller, F.; Borghoite, H.; Stenger, H.; Vogler, S.; Dehniche, K. *Z. Naturforsch., B: Chem. Sci.* **1989**, *44B*, 1524.
(58) Glueck, D. S.; Brough, A. R.; Mountford, P.; Green, M. L. H. *Inorg. Chem.* **1993**, *32*, 1893–1902.
(59) (a) Cheng, B.; Munro, O. Q.; Marques, H. M.; Scheidt, W. R. *J. Am. Chem. Soc.* **1997**, *119*, 10732–10742. (b) Scheidt, W. R.; Lee, Y. J. In *Metal Complexes with Tetrapyrrole Ligands I*; Springer: Berlin/Heidelberg, 1987; Vol. *64*, pp 1−70. (c) Munro, O. Q.; Bradley, J. C.; Hancock, R. D.; Marques, H. M.; Marsicano, F.; Wade, P. W. *J. Am. Chem. Soc.* **1992**, *114*, 7218–7230.

Table 4. Energy Decomposition Analysis of the Bond Energy between the Free-base Porphyrin and $NaPF_6$ Fragments in SAT_{TPP} and SAT_{TMPP}[a]

	energy terms					
	ΔE_{Pauli}	ΔV_{elstat}	ΔE_{oi}	ΔE_{int}	ΔE_{prep}	ΔE
SAT_{TPP}	50.1	−108.8	−48.1	−106.8	31.7	−75.1
SAT_{TMPP}	51.4	−118.9	−49.0	−116.5	32.4	−84.1

[a] Energy values in kJ/mol.

Figure 11. Plot of the $NaPF_6$ 41a fragment orbital.

In SAT_{TMPP} the total attractive interaction (ΔE_{oi} + ΔV_{elstat}) is actually provided for 71% by electrostatic interactions and for 29% by the covalent ones. The electrostatic contribution to the total attractive interaction decreases to 69% in SAT_{TPP}. The larger electrostatic contribution in SAT_{TMPP} can be rationalized in terms of the increased charge density on the porphyrin macrocycle because of the presence of the electron-donating peripheral methoxy groups.

As for the covalent interactions embodied in the ΔE_{oi} term, they mainly consist of porphyrin to $NaPF_6$ charge transfer interactions (polarization being a very minor component). The acceptor orbital is the lowest unoccupied molecular orbital (LUMO; 41a) of the $NaPF_6$ fragment, which is mostly a Na-3s orbital (Figure 11). Three porphyrin molecular orbitals (MOs) are involved in the charge transfer interaction with the $NaPF_6$-LUMO: the TPP 156−158a, and the TMPP 184−186a. These fragment orbitals are mainly localized on the iminic N atoms of the macrocycle, the highest two displaying also some amplitude on the pyrrolic N atoms, as shown in Figure 12, where the plots of the TPP 156−158a MOs are reported. The porphyrin to sodium charge transfer interaction is rather weak because of the energy mismatch between the involved fragment orbitals. As a matter of fact, the charge transferred from the porphyrin fragment orbitals into the $NaPF_6$-LUMO amounts to only 0.1 electrons, regardless of the macrocycle.

Since the total attractive interaction ($\Delta E_{oi}+\Delta V_{elstat}$) is by far larger than the Pauli repulsion, ΔE_{Pauli}, the ΔE_{int} term is strongly stabilizing in both SAT complexes. This term increases (becomes more negative), however, moving from SAT_{TPP} to SAT_{TMPP}, essentially because of the increase of the ΔV_{elstat} term. When we add to the interaction energy the energy needed to deform the separate molecular fragments ($NaPF_6$ and TPP/TMPP) from their

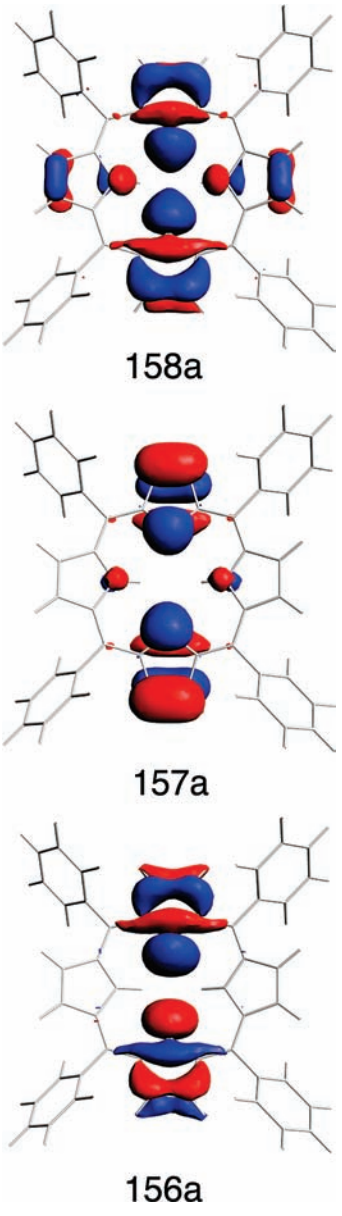

Figure 12. Plots of the 156a, 157a, and 158a TPP fragment orbitals.

equilibrium structure to the geometry they attain in the SAT complexes, we obtain bonding energies that are sufficiently large to guarantee the formation of stable species. The ΔE values reflect, indeed, the predominance of the attractive contribution of the interaction energy term, ΔE_{int}, over the destabilizing ΔE_{prep} term. The latter mostly (∼70%) accounts for the energy cost of the macrocycle deformation (saddling) and is nearly identical in the two SAT complexes.

(d). Ground-State Electronic Structure and Optical Spectra. To provide an interpretation of the UV/vis spectral changes accompanying the formation of the SAT complexes, TDDFT calculations of the electronic absorption spectra have been performed for SAT_{TPP}, SAT_{TMPP}, and the parent free bases. Before dealing with the excited states, the ground-state electronic structure of the SAT complexes will be briefly discussed. To highlight the electronic effects of the sodium-porphyrin interaction, the electronic structures of the parent free bases are

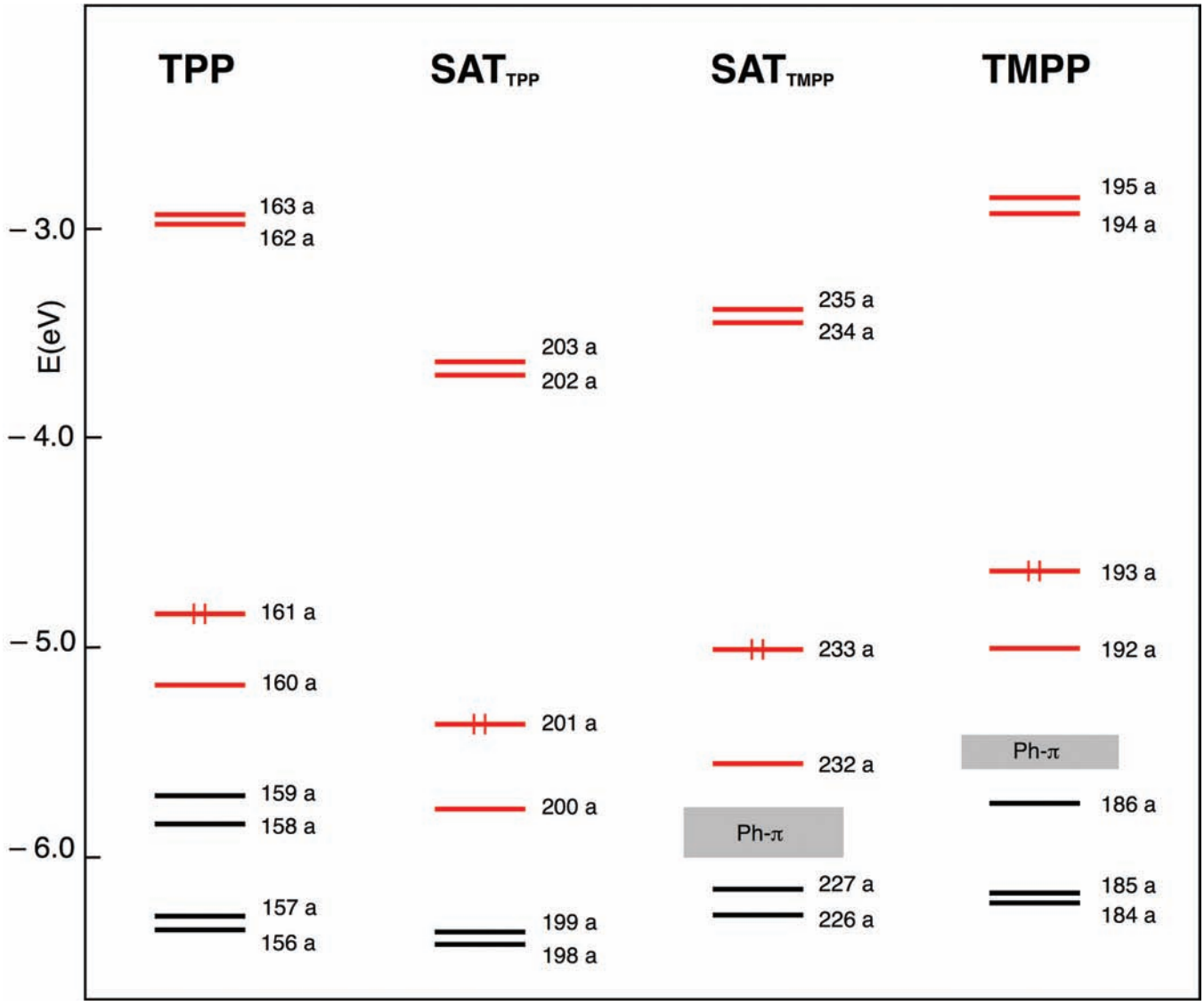

Figure 13. Energy-level scheme for the SAT complexes and their parent free bases obtained at the DFT/BP86/TZVP level. The Gouterman MOs are indicated with red lines.

taken as reference. An energy level scheme of the highest occupied and lowest unoccupied Kohn−Sham orbitals of TPP, SAT_{TPP}, TMPP, and SAT_{TMPP} is shown in Figure 13.

The two highest occupied and two lowest unoccupied MOs in the SAT complexes as well as in the parent free bases are the well-known Gouterman MOs (see the plots of these MOs in Figure 14). Both in SAT_{TPP} and TPP a quite large energy gap separates the lowest occupied Gouterman orbital (HOMO−1) from the lower lying MOs, which are largely localized on the pyrrolenine rings. In SAT_{TMPP} and in TMPP an additional set of π-phenyl orbitals is located between the HOMO−1 and the lower lying pyrrolenine-based MOs. Notably, the TPP 156−158a and TMPP 184−186a MOs are just those involved in the previously discussed charge transfer interactions with $NaPF_6$. Together with the $NaPF_6$-LUMO, these orbitals contribute to the composition of the set of pyrrolenine-based MOs of the SAT complexes, the highest two being shown in the diagram of Figure 13. When comparing the one-electron levels of the SAT complexes to those of the parent free bases, the most remarkable differences consist of the increased HOMO/HOMO−1 splitting and the diminished HOMO/LUMO energy gap, both because of the upshift of the HOMO in the SAT complexes. This upshift is an effect of the π-conjugation between the porphyrin core and the phenyl rings, which is brought about by the saddling-induced twisting of the phenyl rings.[24] Consistent with a larger degree of saddling of the porphyrin ring, the upshift of the HOMO is more pronounced in SAT_{TMPP} than in SAT_{TPP}.

As the electron density on the porphyrin macrocycle decreases upon interaction with $NaPF_6$, a generalized stabilization of the MO levels is observed on going from the free bases to the SAT complexes (Figure 13). This effect incidentally hides the destabilization of the HOMO of the SAT complexes relative to the corresponding free bases.

The changes in the electronic structure associated with the formation of the SAT complexes are reflected in their spectroscopic properties, as shown by the Q-band region that will be discussed first. The excitation energies and

oscillator strengths calculated for the lowest excited states of the SAT complexes and their free-bases are reported in Tables 5 and 6, together with the major one-electron transitions contributing to the excited-state solution vectors. Considering first TPP and TMPP, only two excited states are computed in the energy regime of the Q bands: (i) the 1^1A excited state, accounting for the $Q_x(0,0)$ band, largely described by the HOMO → LUMO transition, and (ii) the 2^1A, responsible for the $Q_y(0,0)$ band, mostly described by the HOMO → LUMO+1 transition. The transitions out of the HOMO−1 into the LUMO and LUMO+1 enter in these states with only a minor weight. The experimental Q_x and Q_y band maxima are satisfactorily reproduced theoretically, although the Q_x/Q_y splitting is somewhat underestimated at both the BP86 and at the B3LYP levels of theory. The absorption wavelengths computed at the B3LYP level are blue-shifted compared to the BP86 values because of the small amount (20%) of the HF exchange present in the B3LYP functional and thereby the increased occupied-virtual gap of the corresponding molecular orbitals. As a result, the Q_x band maximum is better reproduced at the BP86 level, while the Q_y band maximum is more adequately described at the B3LYP level.

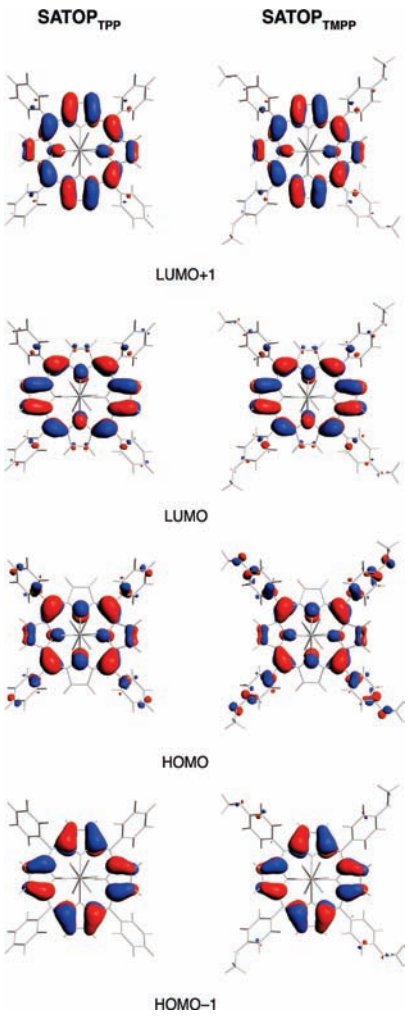

Figure 14. Plots of the SAT_{TPP} and SAT_{TMPP} frontier orbitals.

Also in the case of the SAT complexes only two excited states are predicted in the energy regime of the Q bands, the 1^1A and 2^1A, which share with the 1^1A and 2^1A excited states of the parent free-bases a common electronic origin. TDDFT results show that in the SAT complexes, and especially in SAT_{TMPP}, the 1^1A and 2^1A excited states increase in intensity and shift to longer wavelengths. This latter effect is a consequence of the reduced energy gap between the HOMO and the two nearly degenerate LUMOs upon interaction of TPP/TMPP with $NaPF_6$. In turn, their intensification is related to the increased HOMO/HOMO−1 gap that causes a somewhat smaller mixing of the Gouterman transitions, and hence a less effective cancellation of their large dipole moments. Indeed, the contributions of the transitions out of the HOMO−1 into the LUMO and LUMO+1 to the 1^1A and 2^1A excited states decrease moving from the free bases to the SAT complexes, as can be inferred from the composition of these states reported in Tables 5 and 6. The excitation energy computed for the 1^1A state of SAT_{TPP} allows to safely assign this state to the longest wavelength Q-band (636 nm) in the absorption spectrum of [NaTPP(TFPB)]. By analogy with TPP this band is therefore denoted as $Q_x(0,0)$. As for the 2^1A state, this should be responsible for the $Q_y(0,0)$ band of the SAT complex. However, this band is not clearly discernible in the electronic spectrum of [NaTPP(TFPB)], but it is likely to contribute to the broad and intense band peaking at about 600 nm, together with the first vibrational progression of the $Q_x(0,0)$ band, $Q_x(1,0)$. Indeed, the coalescence of the $Q_y(0,0)$ and $Q_x(1,0)$ bands gives to the Q-band system

Table 5. Composition, Vertical Excitation Energies, *E*, and Oscillator Strengths, *f*, Computed for the Optically Allowed Excited States Responsible for the Q-band region in SAT_{TPP} and TPP at the BP86 and B3LYP Level of Theory

TDDFT/BP86				TDDFT/B3LYP			
state	composition (%)	*E*(eV/nm)	*f*	state	composition (%)	*E*(eV/nm)	*f*
			SAT_{TPP}				
1^1A	201a → 202a (72) 200a → 203a (27)	1.94/638	0.057	1^1A	201a → 202a (73) 200a → 203a (26)	2.02/615	0.077
2^1A	201a → 203a (69) 200a → 202a (29)	2.06/603	0.074	2^1A	201a → 203a (65) 200a → 202a (34)	2.18/569	0.060
			TPP				
1^1A	161a → 162a (70) 160a → 163a (30)	2.00/620	0.028	1^1A	161a → 162a (66) 160a → 163a (33)	2.11/587	0.022
2^1A	161a → 163a (66) 160a → 162a (32)	2.12/585	0.042	2^1A	161a → 163a (63) 160a → 162a (36)	2.26/549	0.035

Table 6. Composition, Vertical Excitation Energies, *E*, and Oscillator Strengths, *f*, Computed for the Optically Allowed Excited States Responsible for the Q-Band Region in SAT_{TMPP} and TMPP at the BP86 and B3LYP Level of Theory

TDDFT/BP86				TDDFT/B3LYP			
state	composition (%)	*E*(eV/nm)	*f*	state	composition (%)	*E*(eV/nm)	*f*
				SAT_{TMPP}			
1^1A	233a → 234a (81) 232a → 235a (18)	1.81/686	0.130	1^1A	233a → 234a (76) 232a → 235a (23)	1.97/628	0.118
2^1A	233a → 235a (80) 232a → 234a (14)	1.91/651	0.187	2^1A	233a → 235a (76) 232a → 234a (24)	2.10/589	0.169
				TMPP			
1^1A	193a → 194a (74) 192a → 195a (25)	1.95/635	0.056	1^1A	193a → 194a (69) 192a → 195a (30)	2.09/594	0.039
2^1A	193a → 195a (73) 192a → 194a (24)	2.05/604	0.087	2^1A	193a → 195a (68) 192a → 194a (32)	2.22/557	0.065

Table 7. Composition, Vertical Excitation Energies, *E*, and Oscillator Strengths, *f*, Computed at the B3LYP Level of Theory for the Optically Allowed Excited States Responsible for the B-Band Region in SAT_{TPP} and TPP

state	composition (%)	*E*(eV/nm)	*f*
	SAT_{TPP}		
3^1A	200a → 203a (56) 198a → 202a (22) 201a → 202a (16)	3.05/407	0.755
4^1A	200a → 202a (61) 201a → 203a (32)	3.09/401	1.290
	TPP		
3^1A	160a → 163a (53) 161a → 162a (23) 158a → 162a (20)	3.10/400	0.848
4^1A	160a → 162a (58) 161a → 163a (33)	3.20/388	1.310

Table 8. Composition, Vertical Excitation Energies, *E*, and Oscillator Strengths, *f*, Computed at the B3LYP Level for the Optically Allowed Excited States Responsible for the B-Band Region in SAT_{TMPP} and TMPP

state	composition (%)	*E*(eV/nm)	*f*
	SAT_{TMPP}		
3^1A	232a → 235a (52) 230a → 235a (17) 233a → 234a (15)	2.95/420	1.122
4^1A	232a → 234a (54) 230a → 234a (16) 233a → 235a (15)	2.98/416	0.619
	TMPP		
3^1A	192a → 195a (58) 193a → 194a (23) 186a → 194a (15)	3.07/404	1.064
4^1A	192a → 194a (56) 193a → 195a (26) 188a → 195a (10)	3.12/398	1.286

of [NaTPP(TFPB)] its peculiar shape. According to the TDDFT results, the shoulder at the blue-edge of the intense band at about 600 nm should have a vibrational origin. Analogously to TPP, this feature can be identified as the first vibrational progression of the $Q_y(0,0)$ band.

A comparison of the absorption spectra of [NaTMPP-(TFPB)] and TMPP reveals that the four Q bands of the free base coalesce in one broadband extending from about 550 to 700 nm. This is most likely due to the conformational inhomogeneity of the system arising from the rotational freedom of the peripheral methoxy groups. As pointed out by the TDDFT results for SAT_{TMPP} in Table 6, the excitation energies computed for the 1^1A and 2^1A excited states are well within the energy window of the broad Q-band profile of [NaTMPP(TFPB)].

Concerning the B band spectral region, its theoretical description is complicated by the presence of non-Gouterman transitions out of the pyrrolenine-based MOs to the unoccupied Gouterman MOs. As these transitions have some charge transfer (CT) character, they involve excitations from localized into delocalized MOs, the well-known CT problem in TDDFT has to be dealt with.[34,60] As a matter of fact, these CT transitions are calculated at far too low energy when using the pure BP86 functional, so they appear either as spurious states or heavily mix with the Gouterman transitions, making very difficult the interpretation of the absorption spectra in this region. In the present case, the use of a hybrid functional with a small fraction of HF exchange, such as B3LYP, is already sufficient to remedy the CT problem of TDDFT. Therefore, only the TDDFT/B3LYP results are reported (Tables 7 and 8) and discussed. These results show that two intense close lying excited states, 3^1A and 4^1A, are located in the energy regime of the B band for both the free bases and the SAT complexes, these excited states being dominated by the Gouterman transitions. The energies and oscillator strengths computed for these states satisfactorily account for the experimental data, well reproducing the observed small red shift and hypochromicity of the B band on going from the free bases to the corresponding SAT complexes.

(e). Emission Spectra. As previously pointed out, the luminescence properties of the SAT complexes are altered significantly as compared to those of the corresponding

(60) (a) Dreuw, A.; Head-Gordon, M. *J. Am. Chem. Soc.* **2004**, *126*, 4007–4016. (b) Gritsenko, O.; Baerends, E. J. *J. Chem. Phys.* **2004**, *121*, 655–660.

(61) (a) Bonar-Law, R. P. *J. Org. Chem.* **1996**, *61*, 3623–3634. (b) Stone, A.; Fleischer, E. B. *J. Am. Chem. Soc.* **1968**, *90*, 2735–2748.

(62) Kano, K.; Fukuda, K.; Wakami, H.; Nishiyabu, R.; Pasternack, R. F. *J. Am. Chem. Soc.* **2000**, *122*, 7494–7502.

(63) Matos Beja, A.; Paixao, J. A.; Ramos Silva, M.; Alte , L.; Rocha Gonsalves, A. M. d. A.; Pereira, M. M.; Pineiro, M. *Z. Kristallogr.* **1999**, *214*, 253–254.

Table 9. Vertical Absorption Energies (E_{va}), Vertical Emission Energies (E_{ve}), and Stokes Shifts Calculated for the S_1 State of the SAT Complexes Compared to the Experimental Data

	E_{va} (nm)		E_{ve} (nm)		Stokes shift (nm)	
	calc.	exp.[a]	calc.	exp.[a]	calc.	exp.[a]
SAT_{TPP}	638	636	684	665	46	29
SAT_{TMPP}	686	~650	738	685	52	~35

[a] CH_2Cl_2 solution, this work.

free bases. In particular, the fluorescence spectra of the SAT complexes show substantial Stokes shifts between $Q_x(0,0)$ absorption and emission (~680 cm^{-1} in [NaTPP(TFPB)] and ~550 cm^{-1} in [NaTMPP(TFPB)]. As confirmed by TDDFT calculations on the model SAT complexes, the observed Stokes shifts are related to changes in the equilibrium geometry of the excited state responsible for the absorption/emission, the S_1 state, with respect to the ground state. Supporting Information, Table S3 collects the optimized geometries of the lowest excited state, and for the sake of comparison, the geometry of the ground state of SAT_{TPP} and SAT_{TMPP}. As can be inferred from this table, the relaxed geometry of the S_1 state (the 1^1A) is characterized by a remarkable increase of the saddling distortion of the macrocycle and by a more acute aryl−porphyrin dihedral angle. The saddling angle, φ, in the 1^1A excited state increases by 11° and 6° in SAT_{TPP} and SAT_{TMPP}, respectively, as compared to the ground state, whereas the aryl−porphyrin dihedral angle, θ, decreases by about 11° in both complexes. The enhancement of the saddling distortion of the macrocycle in the 1^1A excited state can be explained in terms of the increased electron density on the N atoms that induces a more effective porphyrin/$NaPF_6$ interaction. As a matter of fact, in both complexes the Na−N distances are appreciably shorter in the excited 1^1A state than in the ground state (see Supporting Information, Table S3). The vertical absorption and emission energies, and Stokes shifts computed at the BP86 level of theory for SAT_{TPP} and SAT_{TMPP} are reported in Table 9, and compared with the experimental data. These values are in satisfactory agreement with the experimental ones, particularly in the case of the SAT_{TPP}, indicating that the ground and excited state geometries of the SAT complexes are quite accurately modeled.

Concluding Remarks

Since the first report of Fleischer and Wang,[3] a long debate followed in the literature on evidence for the existence or the non-existence of sitting-atop porphyrin complexes. These species are in most cases relatively unstable, and therefore they have been considered as elusive or merely pointed out as chimeras. In this scenario, we have succeeded in detecting and spectroscopically charactering two novel SAT complexes in organic phase. The interplay of low polarity solvents and bulky and weakly coordinating anions favors the stabilization of these new species in which the sodium ion is interacting with the N atoms of the porphyrin core without the concomitant loss of the N−H groups. The theoretical analysis reveals that covalent interactions are consistently involved in the sodium-porphyrin bond energy, even if electrostatics play the major role. In this context, DFT calculations have afforded structural models for the various species, whereas TDDFT calculations have provided an unambiguous interpretation of their absorption and emission properties.

Our report is not intended to be the conclusive step of a long story, rather it opens the way to the preparation of a series of SAT complexes, giving insights into the fundamental understanding of the role of these species in the coordination of metal ions into the porphyrin core.

Acknowledgment. This paper is dedicated in memory of Prof. Raffaello Romeo.We thank MIUR (PRIN 2006-031909_004) for financial support, and Dr. Norberto Micali (IPCF-CNR, Messina, Italy) for fluorescence lifetimes measurements. A.R. and G.R. acknowledge financial support by the Università della Basilicata, Italy (RIL Funds 2006).

Supporting Information Available: Additional spectroscopic data; comparison between the luminescence characteristics of SAT and monoacid TPP derivatives; deconvolution of the UV/vis spectra of the SAT complexes; data for determining the extinction coefficient of NaTFPB; UV/vis absorption and fluorescence titrations of TPP and TMPP solutions in CH_2Cl_2 with NaTFPB; optimized geometrical parameters for the ground and 1^1A excited states of SAT_{TPP} (**A**) and SAT_{TMPP} (**A**); Cartesian coordinates of the optimized structures of SAT_{TPP} (**A**), SAT_{TMPP} (**A**), TPP, TMPP, SAT_{TPP} (**B**), SAT_{TMPP} (**B**), SAT_{TPP} (**A**) 1^1A excited state, SAT_{TMPP} (**A**) 1^1A excited state. This material is available free of charge via the Internet at http://pubs.acs.org.